Preparation and characterization of platinum black electrodes

B. ILIC*, D. CZAPLEWSKI*
Microfabrication Application Laboratories, University of Illinois at Chicago, USA
E-mail: bi22@cornell.edu

P. NEUZIL
Institute of Microelectronics, 11 Science Park Road, Singapore, 117685

T. STANCZYK‡
Microfabrication Application Laboratories, University of Illinois at Chicago, USA

J. BLOUGH
Department of Civil and Materials Engineering, University of Illinois at Chicago, USA

G. J. MACLAY
Microfabrication Application Laboratories, University of Illinois at Chicago, USA

We have investigated properties of electrochemically deposited platinum black by atomic force and scanning electron microscopy. Platinum black was deposited on evaporated platinum electrodes. Deposition time and cure temperature was found to influence the quality and morphology of the platinum black layer. Morphological inclusions were readily observed in films deposited for duration of less than 60 seconds at a bias of 1.5 V against a platinum counter electrode. Shorting of the microfabricated electrodes due to lateral outgrowth of high surface area platinum black was observed when current densities on the order of 100 mA cm^{-2} were employed. We further show that reproducibility of highly adherent platinized electrodes is achieved. © *2000 Kluwer Academic Publishers*

1. Introduction

Platinized electrodes, wherein a high surface area platinum black is formed, have attracted attention in many areas of chemistry, biology and physics [1–7]. Particularly, high surface area noble metal electrodes such as platinized platinum electrodes are used for a large variety of microfabricated solid state, chemical and biological sensors [8–21]. For example, a typical electrochemical sensor is composed of three electrodes: a sensing or working electrode at which the reaction of interest occurs, a reference electrode that keeps the electrical potential of the working electrode constant during the measurement; and an auxiliary or counter electrode for current injection in the electrolyte. In controlled potential experiments, however, a single electrode can serve as both a counter and a reference electrode. This electrode has a double function of passing current and controlling the potential of the working electrode. Pt is generally considered as both an inert metal which does not enter an electrochemical reaction and a catalytic metal that will provide the proper kinetics which increase the rate of chemical reactions. In contrast to Au and Ag, Pt has the advantage that under positive potential bias it is less reactive to Cl^- ions in an electrolyte. Under these conditions Au and Ag electrodes chlorinate. Therefore, Pt electrodes are most commonly utilized in chemical sensing applications.

The primary benefit of platinized electrodes is the increase in the surface area of the catalyst [22–25]. In the case of the microfabricated CO sensor [20], the high surface area Pt black consequently provides more sites for the oxidation of CO to CO_2. As a result, the sensitivity is greatly enhanced. For instance, in contrast to planar platinum and gold electrodes, enhancement to CO sensitivity by a few orders of magnitude was observed using a platinized Pt working electrode. Pt black is also considered as one of the best materials for the oxidation of H_2O_2. It causes a reduction in the H_2O_2 oxidation potential, which consequently increases the operating stability of the biosensor and decreases interference currents [26]. Platinized Pt electrodes have also played a role as a biosensor transducer and a matrix for enzyme immobilization [27].

The goal of this paper is to investigate effects of electrodeposition conditions and annealing on the topography and adhesion of platinized Pt electrodes. Topography is evaluated using tapping mode atomic force microscopy (TMAFM) and scanning electron

* *Present Address*: Department of Applied and Engineering Physics, Cornell University, 212 Clark Hall, Ithaca, NY, USA.
‡ *Present Address*: Molex Incorporated, 2222 Wellington Court, Lisle, IL, USA.

0022–2461 © *2000 Kluwer Academic Publishers*

microscopy (SEM). Methods of fractal analysis were employed to demonstrate the degree of roughness of the platinization.

2. Fabrication

2.1. Substrate preparation

The silicon substrates consisted of three inch, ⟨100⟩, p-doped prime grade wafers with 6–15 Ω cm resistivity. Prior to any processing, the wafers were cleaned in Summa Clean at 40°C under ultrasonic agitation for 20 minutes. Approximately 1 micron of silicon dioxide was thermally grown in wet ambient (pyrogenic steam) at 1100°C for 140 minutes. This layer served as an insulation layer between the doped Si wafer and the subsequent metal layer electrodes. Silicon nitride was also used as an insulating layer. Next, two hundred and fifty nanometers of silicon nitride (Si_3N_4) was deposited in a low pressure chemical vapor deposition (LPCVD) system using a mixture of dichlorosilane (SiH_2Cl_2) and ammonia (NH_3) at a temperature and pressure of 800°C and 250 mTorr respectively.

The Silicon wafers with oxide and nitride along with the alumina substrates were cleaned in acetone for thirty minutes under ultrasonic agitation. This was done primarily to remove any organic contaminants, which generally hinder adhesion of Platinum. They were then cleaned in isopropyl alcohol for thirty minutes under ultrasonic agitation to remove any residual organic contaminants and acetone residue. A thirty-minute deionized water cascade rinse followed to remove any solvent traces. The wafers were further cleaned in a piranha solution (3 : 1 98% H_2SO_4 : 30% H_2O_2) for a duration of 20 minutes. Again, the wafers were rinsed in a deionized water cascade rinse to remove any acid traces and ionic species. Substrates were nitrogen dried and placed into an oven for 1 hour at 150°C in order to dehydrate the substrates, thereby improving adhesion of Pt films to the substrates.

2.2. Platinum film deposition

Following the clean, 1500 Å of Pt was deposited on the substrates by RF sputtering (Fig. 1a). Initially, the substrates were placed into a CVC SC-4000 sputtering vacuum chamber. At a base pressure of $<2 \times 10^{-7}$ Torr, argon (Ar) was introduced to both raise the pressure to 5.5 mTorr and create a RF Ar plasma for sputtering of Pt. A five-minute predeposition at 110 W forward power was carried out in order to stabilize the plasma and clean the Pt target. To achieve better uniformity, the wafers were rotated during the deposition process.

Wafers were then annealed at 650°C for 1 hour in a furnace under nitrogen ambient. Annealing eliminated use of metallic adhesion promoters, which can potentially perturb the electrochemical cell. Generally, adhesion promoters such as chromium or titanium have been found to degrade the sensing performance. Most importantly, annealing was found to be of indispensable significance to the adhesion of Pt to the substrates [28].

2.3. Photolithography

Photolithography was carried out to define the electrode geometry. First, Hexamethyldisilzane (HMDS) was spun at 4000 rpm for 10 seconds to assist photoresist adhesion. Immediately following this spin, Shipley 1818 positive photoresist was spun at 4000 rpm for 30 seconds. The wafers were prebaked on a hotplate at

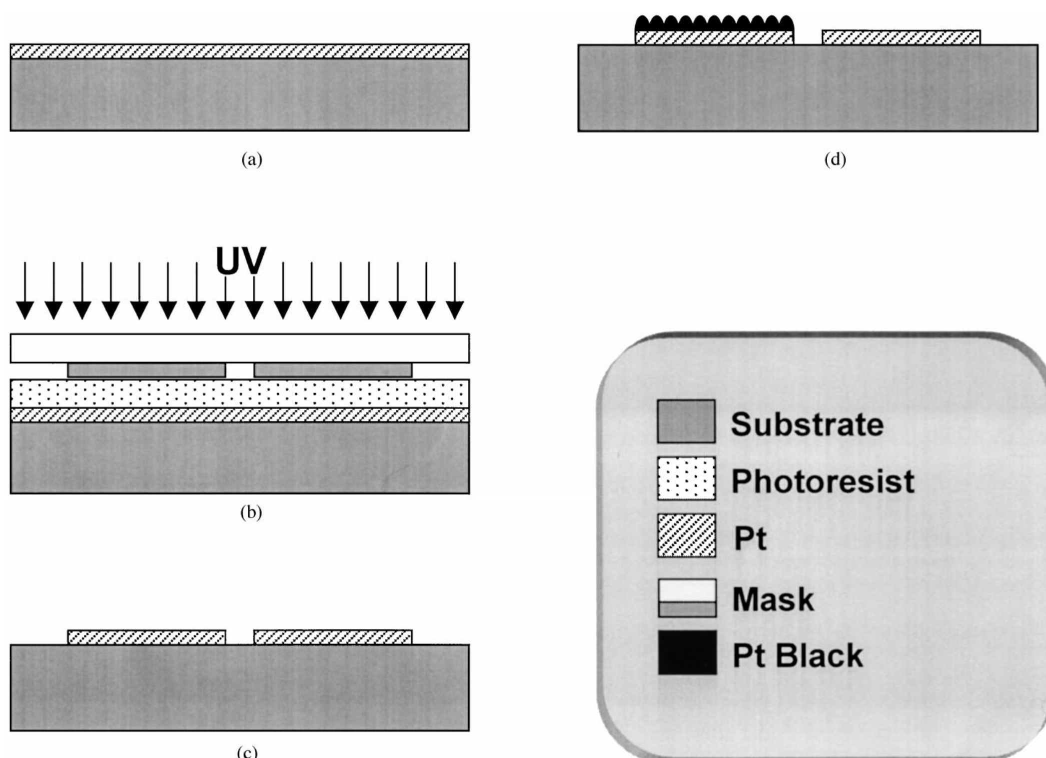

Figure 1 Process flow of the electrode fabrication and platinization. (a) Deposition of 1000 A of platinum via RF sputtering, (b) photolithographic electrode definition, (c) platinum etching using aqua regia, (d) platinization of the platinum working electrode.

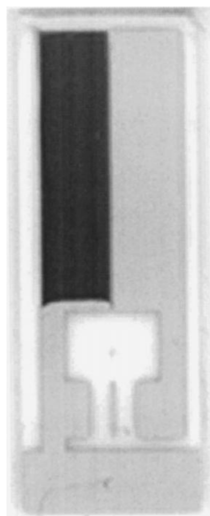

Figure 2 Scanned image of the platinized Pt sensor. The black area over the active portion of the electrode is Pt black while the gray is Pt.

90°C for 5 minutes. Using a Karl Suss contact aligner, the photoresist was exposed to ultra violet light of a mercury lamp through a photomask for 12 seconds at an intensity of 274 W/cm^2 (Fig. 1b). Next, the photoresist was developed in a 1 : 4 solution of Shipley Microposit 351 developer and DI water respectively.

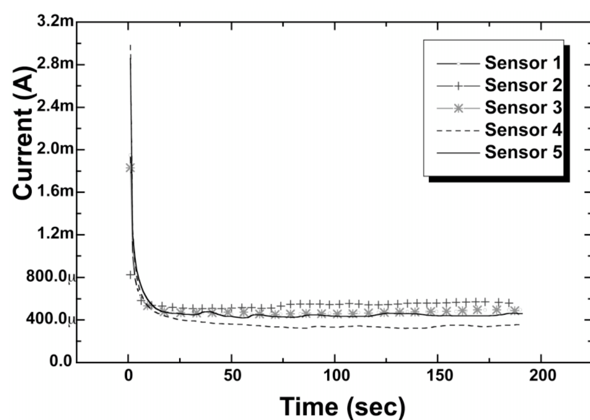

Figure 3 Current versus time characteristics during platinization of 5 sensors.

To ensure resist durability during the Pt etch, the resist was post-baked at 150°C for 60 minutes. Platinum was then etched in a solution of boiling aqua regia for 4 minutes (Fig. 1c). The solution consisted of 550 ml 37% HCl and 30 ml 70% HNO_3 [29]. Finally, photoresist was removed in a piranha solution, mixed to the specifications previously defined. This consequently cleaned the Pt electrodes and the substrate of all contaminants. The substrates were then placed in a deionized water rinse for 30 minutes to remove all acid components.

Following electrode definition, Shipley 1818 was spun on the substrate at 4000 rpm for 30 seconds. Following spinning, the wafers were cured on a hot plate at 90°C for 5 minutes. After curing, they were cut 4 mm wide by 11 mm tall using a dicing saw. The photoresist protected the electrodes from damage during cutting. Following dicing, individual sensors were cleaned in a piranha solution. They were then rinsed in deionized water.

2.4. Platinum black coating

The platenizing solution consisted of 3.5% chloroplatenic acid (Engelhard, Iselin, NJ) and 0.005% lead acetate. The working portion of the sensing electrode was immersed into the platenizing solution in order to electrochemically deposit high surface area platinum black. Against a Pt counter electrode, a constant potential of 1.4 V was applied for 190 seconds (Fig. 1d). This setup worked for single sensor deposition. However, a galvanostatic technique was utilized for batch processes, wherein platinum black is selectively deposited upon a strip of sensors or a whole wafer. Here, a constant current source output 30 mA/cm^2 for 140 seconds. After deposition, Platinum Black was cured at various temperatures in nitrogen ambient. Fig. 2 shows a sensor with platinized electrode.

Fig. 3 shows the current versus time characteristics during the deposition for several sensors. The area under the deposition curve yields the total charge consumed in the electrodeposition process which is proportional to the amount of platinum black deposited on the sensing electrode. Assuming the same deposition

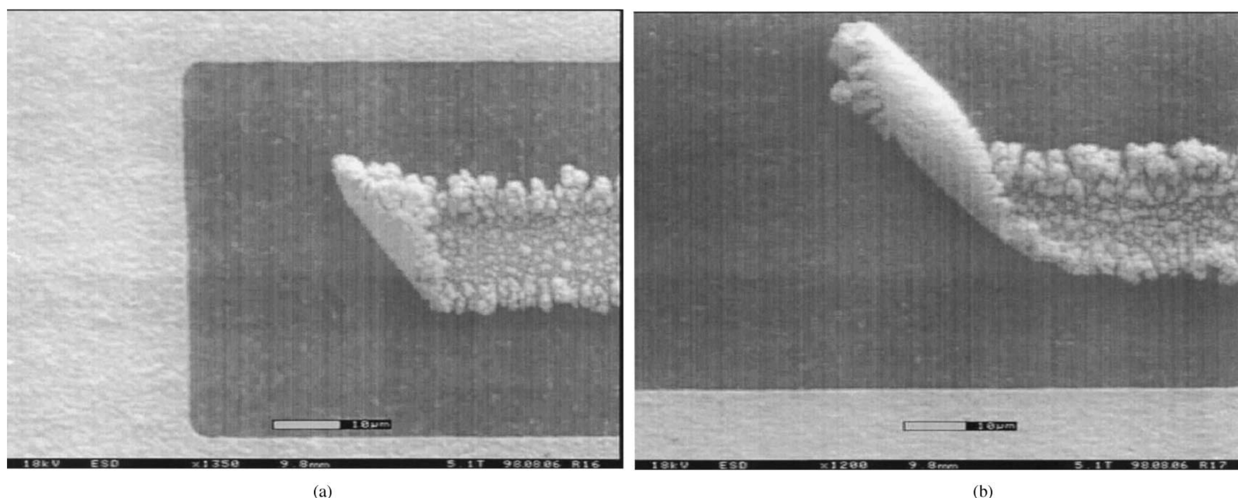

(a) (b)

Figure 4 Scanning electron micrographs showing peeling of platinized electrodes on alumina substrates.

efficiency during each deposition, through numerical integration, variations in the total Pt black deposited were less than 10%. The slight deviation of the platinum black coating was primarily due to the uncontrolled variation of the exposed area due to the immersion depth of the electrode, during electrodeposition.

3. Results and discussion

3.1. Adhesion of platinum

Adhesion of Pt on the substrates is of critical importance for further platinization and sensor fabrication. The adhesion of Pt was found to vary greatly with substrate preparation techniques and different substrates.

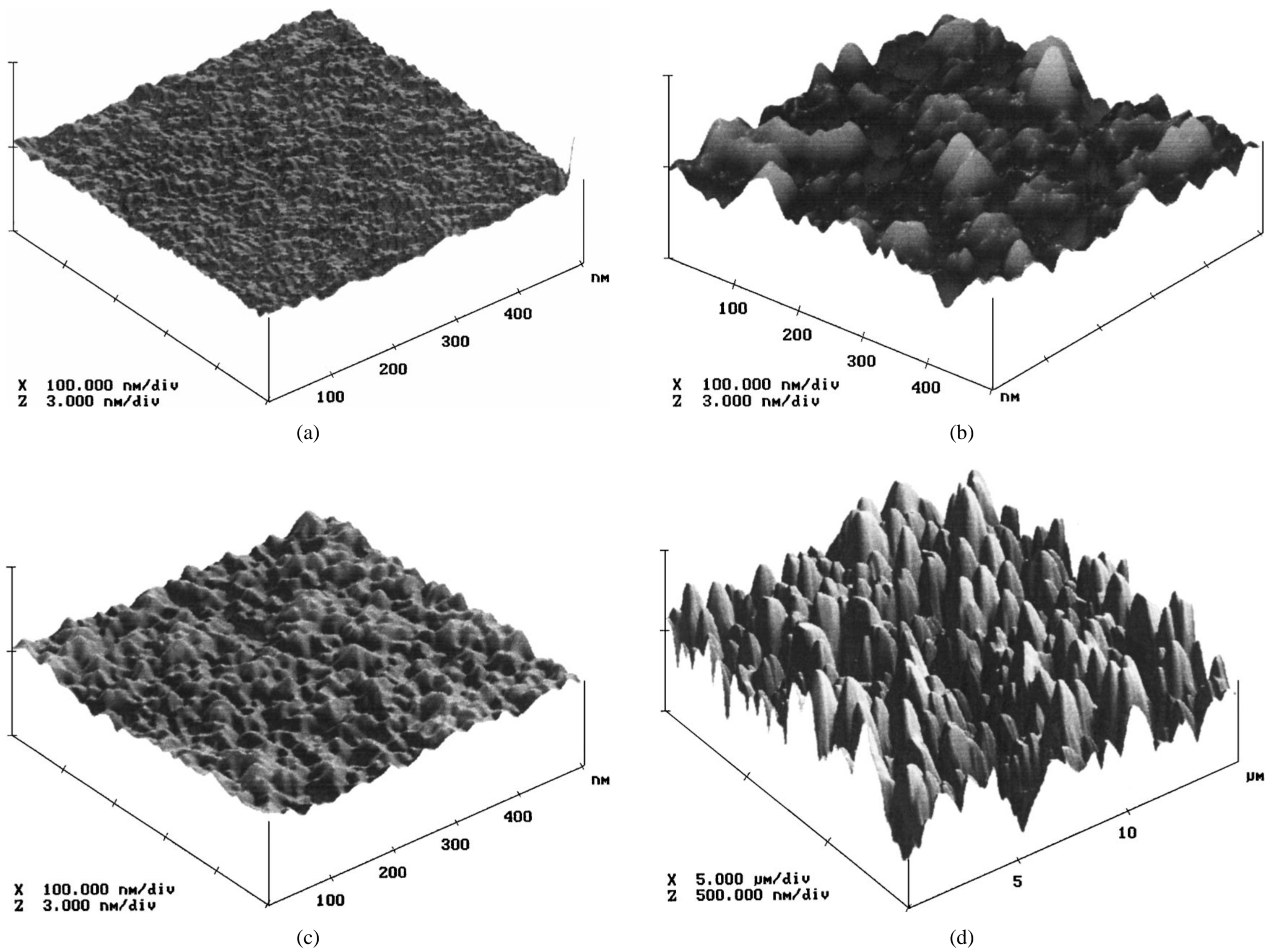

Figure 5 Tapping mode atomic force topographs of various substrates. (a) 500 nm × 500 nm AFM scan of a clean Silicon (100) surface, (b) 500 nm × 500 nm AFM scan of LPCVD silicon nitride, (c) 500 nm × 500 nm AFM scan of an oxidized(100) Si wafer, (d) 15 μm × 15 μm AFM scan of alumina.

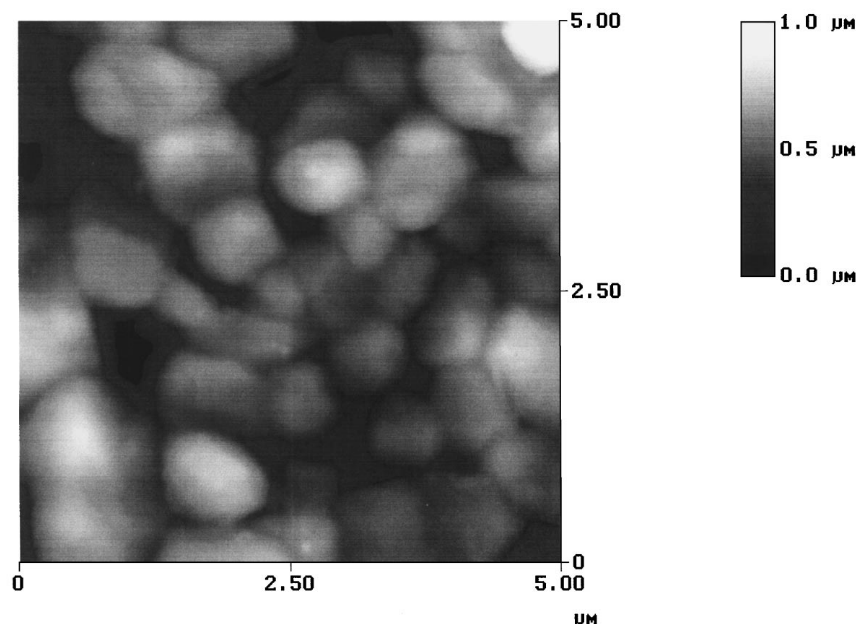

Figure 6 5 μm × 5 μm tapping mode AFM image of sputtered platinum.

Five types of substrates were used: silicon; thin film stoichiometric silicon nitride, low-stress silicon nitride and silicon dioxide on silicon substrates; and alumina. Stoichiometric silicon nitride has a formula of Si_3N_4, while low stress silicon nitride has a higher silicon content, as seen in its formula SiN_x where $x < 4/3$ [30–32]. The biggest difference between the two materials is their chemistry; however, the silicon industry utilizes the two materials because they exhibit differences in stress. The stoichiometric silicon nitride is known to have a much higher stress than the silicon-rich low stress silicon nitride.

The most critical step to ensure good platinum adhesion is the post-sputter cure at 600°C. If the anneal was not carried out, regardless of the substrates or their preparation, Pt would peel during either electrode definition or platinization. To determine initial film adhesion, the standard Scotch® Tape test was performed before any other processing step to rule out other causes of film de-adhesion [33, 34]. It was found that the test would remove Pt from the surface of the wafers, thereby showing poor adhesion following sputtering.

The second critical step to prevent peeling of the Pt film is a pre-sputter dehydration of the substrates. Under air ambient conditions most surfaces will accumulate several monolayers of adsorbed gases such as condensed water vapors, that is why the substrates were placed in a 150°C oven for dehydration following the pre-deposition cleaning. If this step was not carried out, again, the electrodes would peel during electrode

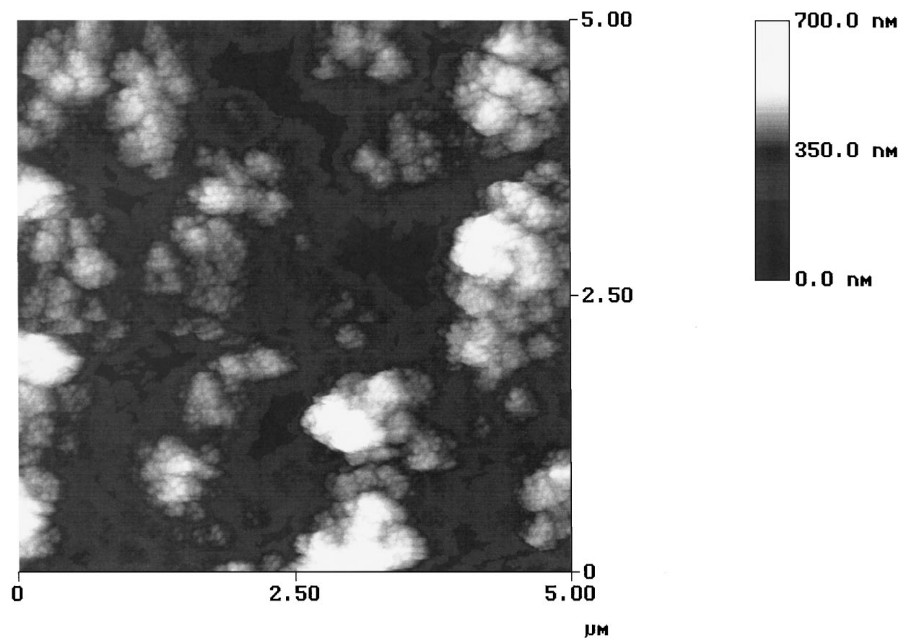

(a)

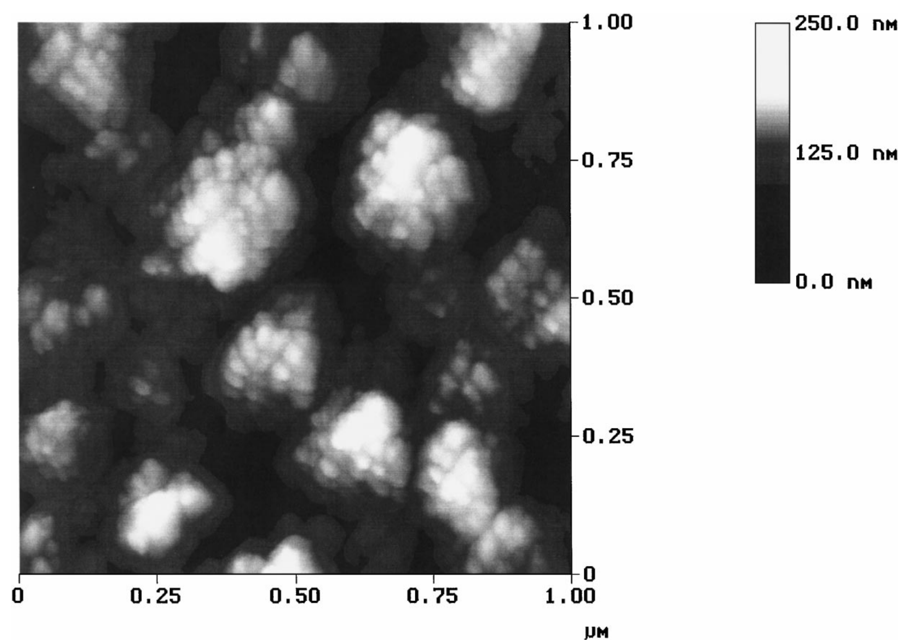

(b)

Figure 7 Tapping mode atomic force topographs of annealed platinized Pt electrodes. (a) uncured (5 μm × 5 μm scan), (b) uncured (1 μm × 1 μm scan), (c) 100°C anneal (5 μm × 5 μm scan), (d) 300°C anneal (5 μm × 5 μm scan), (e) 650°C (5 μm × 5 μm scan). (*Continued*)

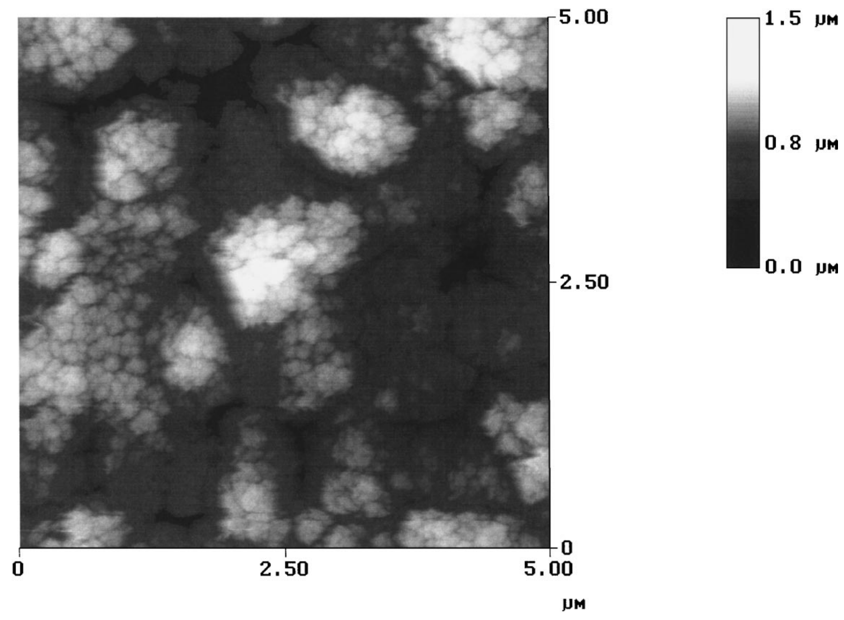

(c)

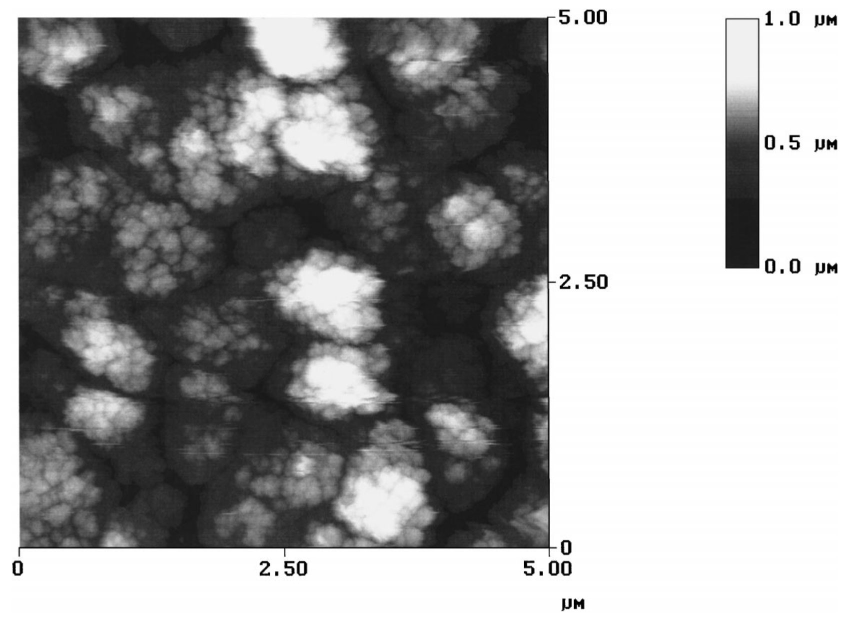

(d)

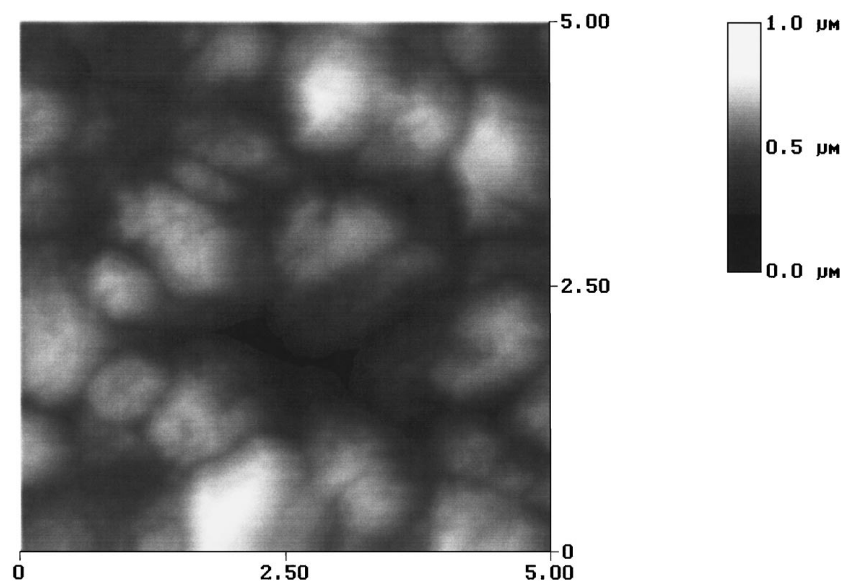

(e)

Figure 7 (*Continued*).

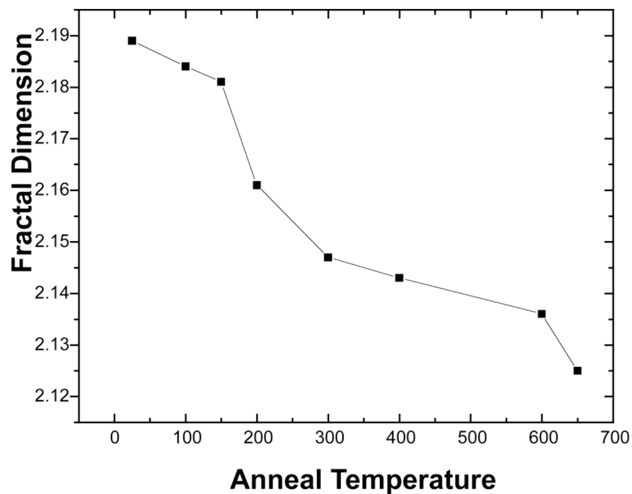

Figure 8 Fractal dimension versus Pt black anneal temperature plot.

definition or platinization. An example of peeling following platinization is shown in Fig. 4a and b.

Generally, to enhance adhesion, it is highly advantageous to include a layer of strong oxide forming element between the substrate and metal. Intermediate adhesion layers such as titanium and chromium are typically used for this purpose. However, it is critical that adhesion layers is not used to aid in the platinum adhesion since layers such as titanium and chromium cause corrosion currents in most applications, which prevent accurate measurements of potentials or currents.

Platinum adhesion also depends on substrate choice. Following adequate surface preparation, cleaning, rinsing, and dehydration, it was observed that platinum did not adhere well to silicon oxide and stoichiometric silicon nitride, because local reactions of the materials did not take place. However, on Si, low-stress silicon nitride

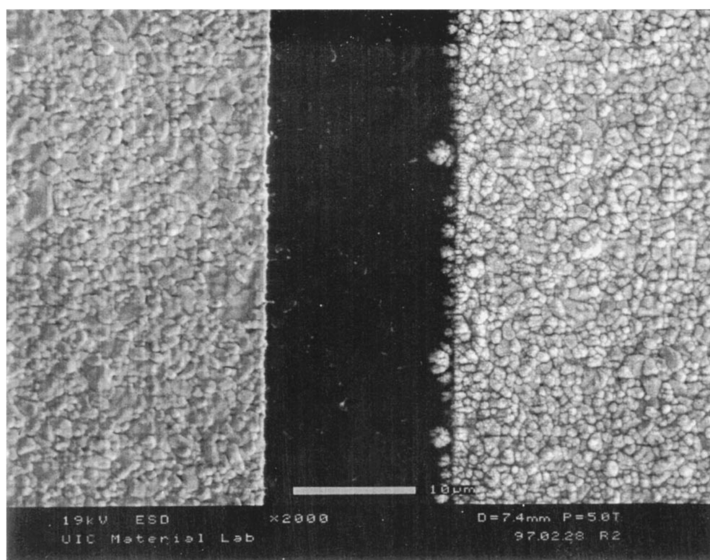

(a)

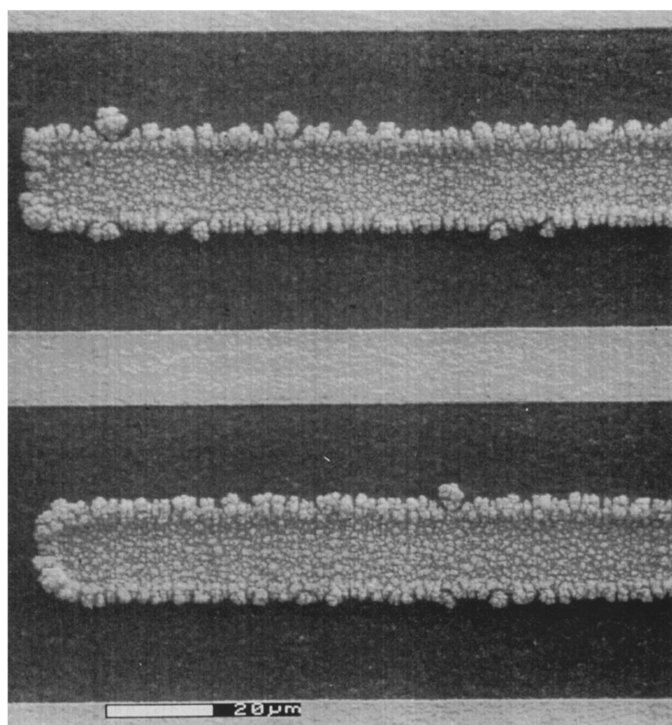

(b)

Figure 9 Scanning electron micrograph of non-uniform lateral outgrowth of platinum black at various magnifications: (a) 2000×, (b) 510× of a 10 μm spacing interdigitated electrode configuration, (c) 1400× of a corner. (*Continued*)

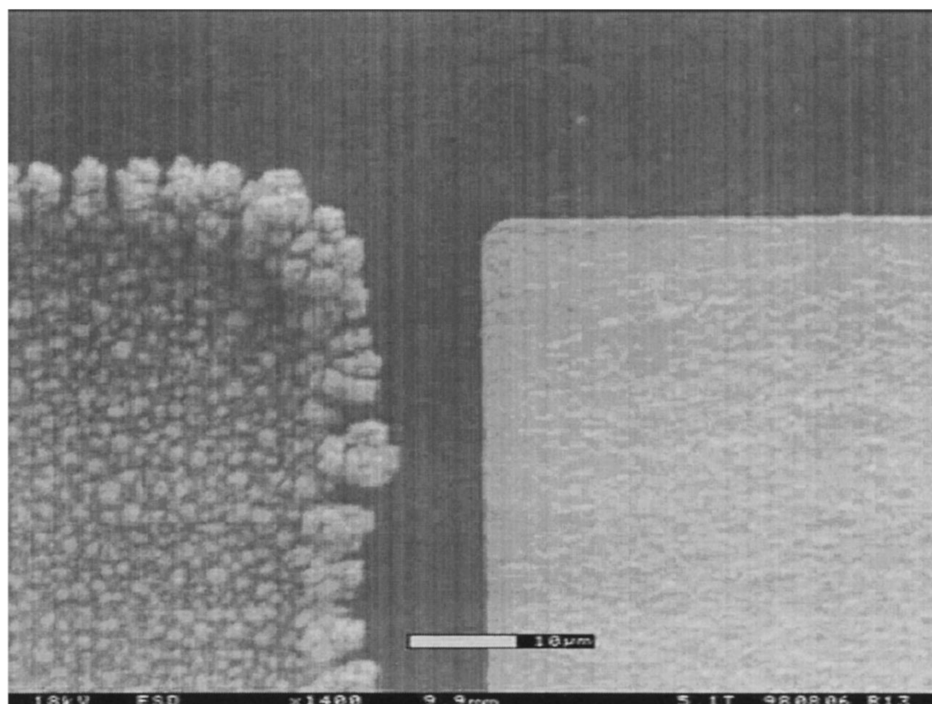

(c)

Figure 9 (*Continued*).

and alumina, properly prepared substrates did not exhibit peeling or other signs of poor adhesion. In the case of Si, it is common that a platinum-silicon compound forms at 600°C, where platinum reacts with silicon to form a platinum silicide (PtSi) at the interface. This is also true for low stress silicon nitride since the layer is silicon rich. However, on the alumina substrates, excellent adhesion was observed due to a high surface roughness. This facilitates mechanical interlocking to take place between Pt and Al_2O_3. Surface roughness did not figure into the adhesion on the silicon, silicon nitride and silicon dioxide surfaces since they are extremely smooth compared with the surface of alumina. From AFM imaging, the RMS roughness for Si, SiO_2, Si_3N_4 were respectively in the range 0.6–0.8 A, 4–6 A, and 8–16 A. Fig. 5a–d shows atomic force micrographs of the surfaces of the substrates, where it is apparent that surface roughness is large for alumina and small for the other substrates.

3.2. Platinized electrodes analysis

3.2.1. Grain size

Platinum black electrodes were evaluated using both atomic force and scanning electron microscopy. Anneals at various temperatures were carried out and the average grain area was determined using an AFM in tapping mode with oxide sharpened silicon tips [35, 36]. Ordinary profilometry and contact mode AFM imaging could not be used to image Pt black since at the lowest force setting it was strong enough to damage the surface. Fig. 6 shows an AFM image of a smooth platinum surface prior deposition while Fig. 7a–e show AFM images of platinum black films cured at several temperatures. Tapping mode AFM images show a randomly scattered nanogranular structure of which the cauliflower platinized structure is composed. In particular, Fig. 7b shows an 1×1 μm AFM topograph of an uncured platinized film. Grains on the order of tens of nanometers are seen. These nano-sized grains coalesce to form larger grains at elevated cure temperatures and almost completely disappear when the curing temperature is above 650°C (Fig. 7e). Therefore, from the AFM images, it is apparent that the higher the cure temperature the larger the resulting grain size. This further implies that at higher cure temperatures the surface area is lowered.

3.2.2. Fractal imaging

Fractal dimension analysis can be used to mathematically characterize the geometric complexity of the surface. The fractal dimension of a three dimensional surface varies from a minimum of 2.00 for a flat surface to a maximum of 3.00 for an infinitely rough surface. Digital Instruments software utilizes an algorithm which comprises of a triangular form of analysis [37]. Fig. 8 shows a plot of the fractal dimension versus the Pt black curing temperature. The dependence of fractal dimension decreases with increasing Pt black cure temperature which alternatively signifies a decrease in both roughness as well as surface area with increasing cure temperature. This is because higher anneal temperatures result in an increased surface mobility which leads to filling of the peaks and the valleys, thereby decreasing the surface roughness.

3.3. Deposition time during platinization

Deposition time, during platinization, was found to be important factor for the uniformity and adhesion of platinum black. From Fig. 9a–c, non-uniform

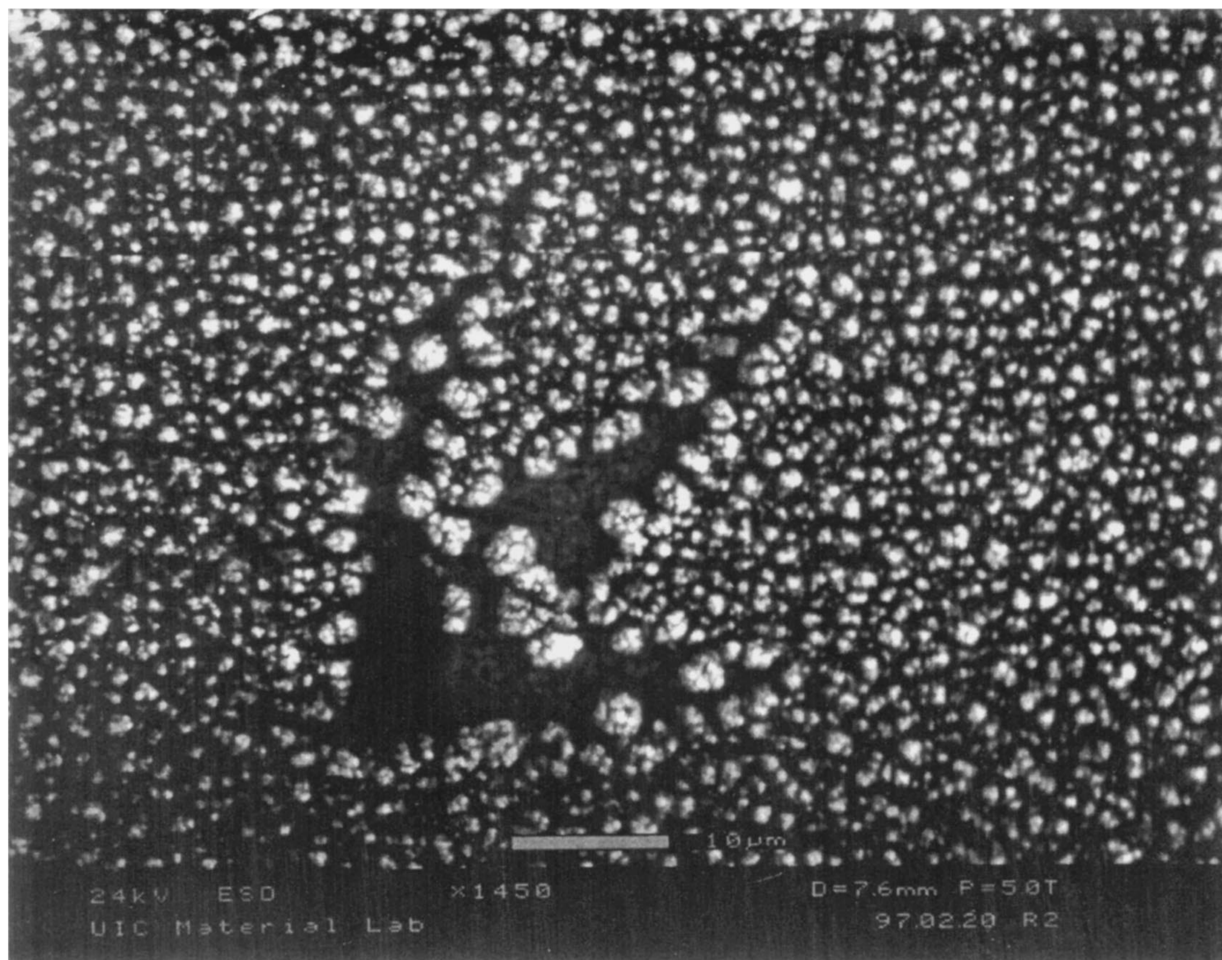

Figure 10 Scanning electron micrograph at 1450× of voids in Pt black.

outgrowth of platinum black for several geometries was shown to be on the order of a few microns for deposition current densities greater than 100 mA cm^{-2}. Also, even at low fields, shorting of the 20 μm gap electrodes was readily observed for deposition times exceeding 10 minutes. This is primarily due to a large electric field concentration at the edge of the planar electrode. From, the Appendix A derivation of the field at the corner of our electrodes, Equations A.4a and A.4b show electric field line crowding at the edge which is synonymous with a local increase in the electric field that is responsible for lateral outgrowth.

Voids, as shown in Fig. 10, on the order of several micrometers were observed throughout the electrode when the deposition time was less than 60 seconds. The size and distribution of the voids were random. This is a consequence of a nonhomogeneous nature of the platinum black deposition process. Since the observed lateral encroachment is on the order of the void-size, given enough time, lateral encroachment will eventually close the gap.

4. Conclusions

Atomic force and scanning electron microscopy were used to investigate the topography of annealed microfabricated platinized Pt electrodes. Surface properties of the electrochemically prepared high surface area Pt black films were found to have a strong dependence on electrode preparation prior electrodeposition. Scotch tape tests showed stoichiometric silicon nitride and silicon dioxide to exhibit poor adhesion. On the other hand, Si, low stress silicon nitride and alumina substrates showed excellent adhesion. Si, SiO_2 and Si_3N_4 substrates are relatively smooth and in order for adhesion to take place an intermetallic platinum silicide forms. It is known that oxide and stoichiometric nitride do not form silicides with Pt. However, due to the high silicon concentration in the low stress Si_3N_4, it is possible that a Pt-silicide was formed and thus enhanced adhesion.

Initial surface roughness of the substrate was also found to affect the adhesion of the electrodes. Increased surface roughness may promote adhesion because the substrate exhibits more surface area than a flat surface, and mechanical interlocking between the substrate and film may occur as in the case of alumina. Adhesion also depends upon the cleanliness of the substrate. Contamination generally results in reduced adhesion, as does an adsorbed gas layer. A dehydration treatment was found to be essential in order to remove any adsorbed water vapors. Cleaning the substrate prior deposition was important to assure film adhesion. Platinum black electrodes generally exhibit morphological anomalies that are alleviated by a piranha pretreatment.

Deposition time played an important role for the uniformity and adhesion of Pt black. Non uniform outgrowth of platinum black was shown to be on the order

of a few microns for deposition current densities in access of 100 mA cm^{-2}. The lateral outgrowth was due to the electric field line crowding at the edge of the electrodes. Therefore, we can see that excessive protrusions of platinum black can play a major role when considering electrode spacing ranging from a few to tens of micrometers. On the other extreme end of the spectrum, when the deposition time is sufficiently short (<60 seconds), large voids were readily seen throughout the electrode due to possible passivating contaminants.

Finally, we have used AFM of the platinized working electrode toshow a direct cure temperature correlation with respect to the average grain size. Larger grains were observed for higher anneal temperatures.

Appendix A: Electric field crowding observed at corners

Consider an intersection of two conducting planes held at a potential V, as shown in Fig. A1, that define a corner in two dimensions with an opening angle α. In the polar coordinate system (ρ, ϕ), Laplace's equation in two-dimensions is given by,

$$\frac{1}{\rho}\frac{\partial}{\partial\rho}\left(\rho\frac{\partial\Phi}{\partial\rho}\right)+\frac{1}{\rho^2}\frac{\partial^2\Phi}{\partial\phi^2}=0 \qquad \text{(A.1)}$$

where the general solution may be expressed as,

$$\Phi(\rho,\phi)=V+\sum_{l=1}^{\infty}a_1\rho^{\frac{l\pi}{\alpha}}\sin\left(\frac{l\pi\phi}{\alpha}\right) \qquad \text{(A.2)}$$

For small enough ρ only the first term in the series becomes important, therefore near $\rho=0$ the potential is approximately,

$$\Phi(\rho,\phi)\cong V+a_1\rho^{\frac{\pi}{\alpha}}\sin\left(\frac{\pi\phi}{\alpha}\right) \qquad \text{(A.3)}$$

The electric field components are given by,

$$E_\rho(\rho,\phi)=-\frac{\partial\Phi}{\partial\rho}=-\frac{\pi a_1}{\alpha}\rho^{\left(\frac{\pi}{\alpha}\right)-1}\sin\left(\frac{\pi\phi}{\alpha}\right) \qquad \text{(A.4a)}$$

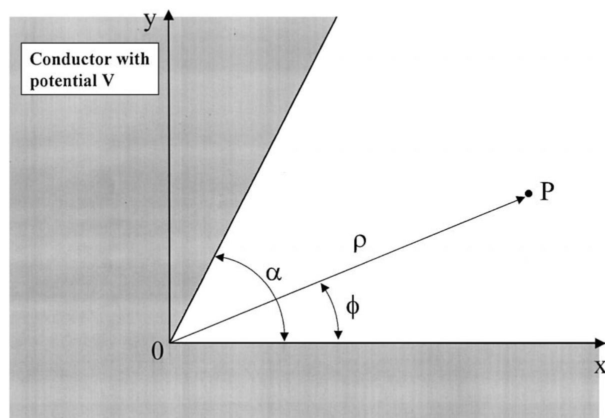

Figure A1 Intersection of two conducting planes held at a potential V.

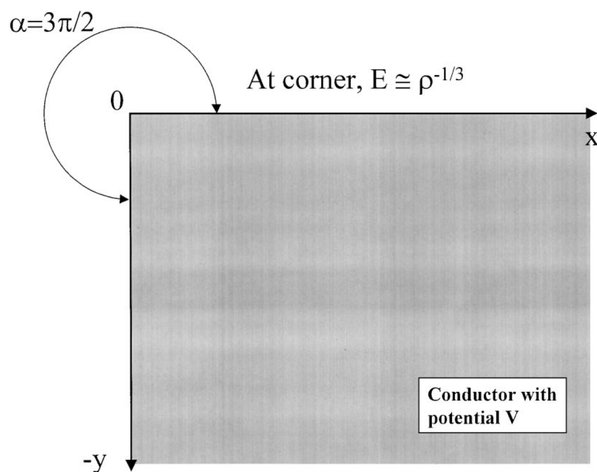

Figure A2 Special case of the opening angle producing an outside corner.

$$E_\phi(\rho,\phi)=-\frac{1}{\rho}\frac{\partial\Phi}{\partial\phi}=-\frac{\pi a_1}{\alpha}\rho^{\left(\frac{\pi}{\alpha}\right)-1}\cos\left(\frac{\pi\phi}{\alpha}\right) \qquad \text{(A.4b)}$$

The case of $\alpha=3\pi/2$ is shown in Fig. A2. At this angle the corner becomes an edge, as in the case of our electrodes, where the field becomes singular as $\rho\to 0$.

Acknowledgements

The authors would like to acknowledge F. Michael Serry (Digital Instruments, Santa Barbara CA) and Tony Cocco (University of Illinois) for their helpful discussions. The authors would further like to thank Clark E. Smith, Ed Duran, and Mark Devine at First Alert for their support and Jiri Holoubek from IST AG, Switzerland for useful hints regarding the Pt deposition and treatment.

References

1. W. M. MacNEVIN and M. LEVITSKY, *Anal. Chem.* **24** (1952) 973.
2. W. LANG, K. KUHL and H. SANDMAIER, *Sens. Act. A* **34** (1992) 243.
3. B. WRIGHT and E. B. PATTINSON, *J. Phys. D: Appl. Phys.* **7** (1974) 1560.
4. J. R. LOSEE and D. S. BURCH, *Rev. Sci. Inst.* **43** (1972) 146.
5. J. J. RUSH, R. R. CAVANAGH and R. D. KELLEY, *J. Vac. Sci. Technol. A* **1** (1982) 1245.
6. F. C. ANSON and D. M. KING, *Anal. Chem.* **34** (1962) 362.
7. F. C. ANSON, *ibid.* **33** (1961) 934.
8. J. J. PANCRAZIO, R. P. BEY, A. LOLOEE, S. MANN, H. C. CHAO, L. L. HOWARD, W. M. GOSNEY, D. A. BORKHOLDER, G. T. A. KOVACS, P. MANOS, D. S. CUTTINO and D. A. STENGER, *Biosensors and Bioelectronics* **13** (1998) 971.
9. S. YAMAUCHI, M. YAOITA, F. MATSUMOTO, T. YOKOYAMA and Y. IKARIYAMA, *Sens. Act. B* **13** (1993) 79.
10. K. W. JOHNSON, *ibid.* **5** (1990) 85.
11. R. B. BEARD, J. F. DeROSA, R. M. KOERNER, S. E. DUBIN and K. J. LEE, *IEEE Trans. Biomed. Engin.* **19** (1972) 233.
12. T. SUDA and S. UENO, *J. Appl. Phys.* **85** (1999) 5711.

13. D. R. JUNG, D. S. CUTTINO, J. J. PANCRAZIO, P. MANOS, T. CLUSTER, R. S. SATHANOORI, L. E. ALOI, M. G. COULOMBE, M. A. CZARNASKI, D. A. BORKHOLDER, G. T. A. KOVACS, P. BEY, D. A. STENGER and J. J. HICKMAN, *J. Vac. Sci. Technol. A* **16** (1998) 1183.
14. R. J. REAY, R. DADOO, C. W. STORMENT, R. N. ZARE and G. T. A. KOVACS, in 1994 Solid State Sensors and Actuators Workshop, June 13–16, Hilton Head, South Carolina, 1994.
15. S. R. SAMMS, S. WASMUS and R. F. SAVINELL, *J. Electrochem. Soc.* **143** (1996) 1498.
16. J. KUWANO, A. WAKAGI and M. KATO, *ibid.* **139** (1992) L113.
17. T. OYABU, T. OSAWA and T. KUROBE, *J. Appl. Phys.* **53** (1982) 7125.
18. R. V. KUMAR and D. J. FRAY, *Sens. Act.* **15** (1988) 185.
19. P. VANYSEK, *Can. J. Chem.* **75** (1997) 1635.
20. G. J. MACLAY, D. KEYVANI and S. B. LEE, in Proceedings of the Second International Symposium on Microstructures and Microfabricated Systems, Chicago, October 1995 (Electrochemical Society Proceedings) Vol. 95-27, p. 177.
21. S. B. LEE, A. COCCO, D. KEYVANNI and G. J. MACLAY, *J. Electrochem. Soc.* **142** (1995) 157.
22. T. BIEGLER, *ibid.* **116** (1969) 1131.
23. M. J. JONCICH and N. HACKERMAN, *ibid.* **111** (1964) 1286.
24. C. A. MARRESE, *Anal. Chem.* **59** (1987) 217.
25. A. M. FELTHAM and M. SPIRO, *Chem. Rev.* **71** (1971) 177.
26. G. F. KHAN and W. WERNET, *J. Electrochem. Soc.* **143** (1996) 3336.
27. Y. IKARIYAMA, S. YAMAUCHI, T. YUKIASHI and H. USHIODA, *ibid.* **136** (1989) 702.
28. J. HOLOUBEK, private communication.
29. P. W. H. WALKER, TERRIN (eds.), “Handbook of Metal Etchants” (CRC Press, 1991).
30. S. L. ZHANG, J. T. WANG and W. KAPLAN, *Thin Solid Films* **213** (1992) 182.
31. T. MAKINO, *Solid State Sci. and Technol.* **130** (1983) 450.
32. S. HABERMEHL, *J. Appl. Phys.* **83** (1998) 4672.
33. P. A. STEINMANN and H. E. HINTERMANN, *J. Vac. Sci. Technol.* **A7** (1989) 2267.
34. J. VALLI, *ibid.* **A4** (1986) 3007.
35. R. W. STARK, T. DROBEK and W. M. HECKL, *Appl. Phys. Lett.* **74** (1999) 3296.
36. A. KUHLE, A. H. SORENSEN and J. BOHR, *J. Appl. Phys.* **81** (1997) 6562.
37. Digital Instruments Nanoscope III Command Reference Manual.

Received 5 October
and accepted 14 December 1999